Available online at www.sciencedirect.com
ScienceDirect
Journal of Power Sources 160 (2006) 933–939
JOURNAL OF POWER SOURCES
www.elsevier.com/locate/jpowsour

The stability of a PtRu/C electrocatalyst at anode potentials in a direct methanol fuel cell

Weimin Chen [a], Gongquan Sun [a], Zhenxing Liang [a], Qing Mao [a], Huanqiao Li [a], Guoxiong Wang [a], Qin Xin [a,*], Hyuk Chang [b], Chanho Pak [b], Doyoung Seung [b]

[a] *Direct Alcohol Fuel Cell Laboratory, Dalian Institute of Chemical Physics, Chinese Academy of Sciences, Dalian 116023, China*
[b] *Fuel Cell Program Team, Samsung Advanced Institute of Technology, San 14-1, Nongseo-Ri, Kihung-Eup, Yongin, Kyungki-Do 449-712, South Korea*

Received 28 December 2005; received in revised form 14 February 2006; accepted 14 February 2006
Available online 29 March 2006

Abstract

Potential-scan tests were conducted to evaluate the stability of a PtRu/C electrocatalyst at anode potentials in a direct methanol fuel cell (DMFC). The results show that, under normal operating conditions, the anode potential in a DMFC is benign for the PtRu/C electrocatalyst. But in the case of deep discharge or short circuit, the anode potential value may exceed 0.6 V versus DHE, which is harmful to the PtRu/C electrocatalyst. The dissolution of catalyst components results in an enhanced ohmic resistance and a lowered catalytic activity for methanol electro-oxidation.

Keywords: Direct methanol fuel cell (DMFC); Potential scan; Stability; PtRu/C; Electrocatalyst

1. Introduction

The direct methanol fuel cell (DMFC) is a promising portable power source due to its merits such as high energy efficiency, ambient operating conditions and potentially good portability [1–4]. For commercial applications, a lifetime of thousands of hours is necessary. In this regard, the stability of the electrocatalysts is very important. Long-term operations of the fuel cell often cause degradation of the electrocatalysts, including the dissolution of catalyst components and the agglomeration of catalyst particles. The anodic potential is considered to be one of the most important factors that influence the rate and degree in the catalyst-degrading process. For low-temperature fuel cells, such as the polymer electrolyte membrane fuel cell (PEMFC) and the DMFC, the influence of the cathode potential on the degradation of electrocatalysts has been widely studied [5–7]. But in the case of the anode, relevant work is scarce [8]. This is mainly because the anode potential value is much lower than the cathode, so its influence is limited. But with respect to long-term operation of a DMFC, this influence should not be neglected. The typical anode electrocatalyst in a DMFC is a Pt-Ru binary metal electrocatalyst. Compared with platinum, ruthenium is much more unstable in the fuel cell environment. Taniguchi et al. [9] observed ruthenium loss under cell reversal conditions. Piela et al. [10] found ruthenium crossover from the anode side to the cathode side through the membrane during long-term operations. So an investigation of the stability of the PtRu electrocatalyst under anode potential of DMFC is of significance.

The anode potential in the DMFC for the methanol electro-oxidation reaction on the PtRu electrocatalyst, at open circuit, is approximately 0.2 V versus dynamic hydrogen electrode (DHE) at 70–80 °C [11,12], and when the fuel cell operates under normal conditions, the anode potential value is in the range of 0.3–0.5 V [13]. But occasionally, the fuel cell may experience deep discharging processes or even a short circuit, and the anode potential value may reach 0.6 V or even as high as 0.7 V. To investigate the influence of the anode potential on the stability of the PtRu electrocatalyst, in this work, potential-scan tests were conducted in potential regions of 0.2–0.5 V, 0.2–0.6 V and 0.2–0.7 V, respectively. Electrochemical and physical character-

* Corresponding author. Tel.: +86 411 84379071; fax: +86 411 84379071.
E-mail address: xinqin@dicp.ac.cn (Q. Xin).

0378-7753/$ – see front matter © 2006 Elsevier B.V. All rights reserved.
doi:10.1016/j.jpowsour.2006.02.069

izations were performed to study the electrocatalyst degradation after potential scans.

2. Experimental

2.1. Electrode preparation

The anode electrocatalyst studied in this work was a commercial 30 wt.% Pt–15 wt.% Ru/C HiSPEC7000 catalyst (Johnson Matthey, UK). A commercial 40 wt.% Pt/C HiSPEC4000 catalyst (also Johnson Matthey, UK) was applied to the cathode, and served as a counter/reference electrode. The solid electrolyte is a commercial Nafion® 117 perfluorosulfonate ionomer membrane (DuPont Corp.), which was firstly boiled in 0.5 mol L^{-1} sodium hydroxide solution for 1 h, to convert the H^+ form of solubilized membrane into the Na^+ form. The electrocatalyst and 5 wt.% Nafion® ionomer solution (EW = 1100, DuPont Corp.) were ultrasonically mixed in an ethanol solution to form a homogeneous catalyst suspension. A decal method [14] was adopted to make the catalyst coated membrane (CCM). The anode and cathode catalyst layers were hot-pressed onto both sides of a piece of Nafion® 117 membrane, respectively, at 190 °C for 90 s. The catalyst metal loading was 2 mg cm^{-2} for the anode and 1 mg cm^{-2} for the cathode, and the Nafion® ionomer content in the catalyst layers was 15 wt.% for the anode and 10 wt.% for the cathode. The CCM was boiled in a 0.5 mol L^{-1} H_2SO_4 solution for 1 h to reconvert the membrane into the H^+ form.

Vulcan XC-72 carbon black (Cabot Corp.) was suspended in ethanol and the slurry was spread onto Teflon-containing (30 wt.% for cathode, 10 wt.% for anode) carbon papers (SGL Corp.) to form diffusion layers. The loading of the carbon black was 4 mg cm^{-2} for the anode and 3 mg cm^{-2} for the cathode.

The membrane electrode assembly (MEA) was formed by hot-pressing the anode and cathode diffusion layers onto the corresponding sides of the CCM at 135 °C, for 60 s.

2.2. Potential-scan test

Potential-scan tests were carried out at 75 °C, using a single testing cell that made of 316 L stainless steel, with an active cross-sectional area of 4 cm^2. The anode chamber was fed with deionized water, with the flow rate of 1 mL min^{-1}. The cathode served as both counter and reference electrodes, which was fed with humidified hydrogen at 0.1 MPa pressure, and defined as a dynamic hydrogen electrode (DHE). All potential values presented in this work are referred to DHE.

Potential-scan tests were conducted in the potential regions of 0.2–0.5 V, 0.2–0.6 V and 0.2–0.7 V, respectively, with the scan rate of 20 mV s^{-1} and a cycle number of 2000 for each region.

2.3. Electrochemical characterization

Cyclic voltammograms were obtained using a potentiostat/galvanostat (EG&G Model 273A). For the cyclic voltammetry (CV) measurement, the anode chamber was fed with deionized water, and CV curves were recorded within the potential range of 0–0.7 V, with a scan rate of 20 mV s^{-1}.

For the methanol-stripping test, the anode chamber was fed with 1 mol L^{-1} methanol solution for 10 min, with the anode potential held at 0.1 V. Then the anode chamber was washed with deionized water with a flow rate of 4 mL min^{-1} to remove un-adsorbed methanol molecules, while the anode potential was held at 0.1 V. After 20 min, CV curves were recorded within the potential range of 0.1–0.7 V, with the scan rate of 20 mV s^{-1}. The first and third cycles were recorded.

For a CO-stripping test, the anode was fed with humidified CO/Ar (5 vol.%) gas at 150 mL min^{-1} flow rate and a 0.1 MPa pressure for 30 min, with the potential held at 0.1 V. Then the CO/Ar (5 vol.%) gas was replaced with high-purity nitrogen, while the potential was still held at 0.1 V. After 10 min, CV curves were recorded within the potential range of 0.1–0.7 V, with a scan rate of 20 mV s^{-1}. The first and third cycles were recorded.

Electrochemical impedance spectra (EIS) were measured using a lock-in amplifier (EG&G model 5210) coupled to a potentiostat/galvanostat (EG&G model 273A). Impedance spectra were recorded at 10 points per decade by superimposing a 10 mV ac signal on the cell under potentiostatic mode over the frequency range from 5 kHz to 0.1 Hz.

2.4. Physical characterization

After potential-scan test, the CCM was treated with liquid nitrogen and cut into small pieces for subsequent X-ray diffraction (XRD), transmission electron microscopy (TEM) and energy dispersive X-ray spectroscopy (EDX) analyses.

TEM investigation was carried out using a JEOL JEM-2000EX microscope operating at 120 kV. The size distribution and the mean particle size of the electrocatalyst were obtained by measuring more than 300 particles from TEM images. XRD measurements were performed on a Rigaku X-3000 X-ray diffractometer using Cu Kα radiation with a Ni filter. The tube voltage was maintained at 40 kV, and tube current at 100 mA. The 2θ angular region between 20° and 85° was explored at a scan rate of 5° min^{-1}, with the resolution of 0.02°. The Pt (2 2 0) peak (64–72°) was scanned at 1° min^{-1} to obtain the catalyst particle sizes. Energy dispersive X-ray (EDX) analysis was carried out by an EDX detector combined with a scanning electron microscopy (Philips Model XL-30).

3. Results and discussion

CV curves obtained before and after potential scans are shown in Fig. 1. Two noticeable changes have been observed after potential scans. Firstly, from the inset of Fig. 1, it is seen that, after potential scan in 0.2–0.6 V and 0.2–0.7 V regions, especially for the latter, the hydrogen-desorption peak moved to the right to some extent. For a Ru-rich PtRu surface, the hydrogen-desorption peak appears in a low-potential region [15–21]. So the right-shift of the hydrogen-desorption peak may be due to the loss of ruthenium from the electrocatalyst surface under electrochemical stress. Secondly, the double-layer capacitance (shown in the potential range of 0.4–0.6 V) tends to decrease with the extending scan region. This tendency also became prominent

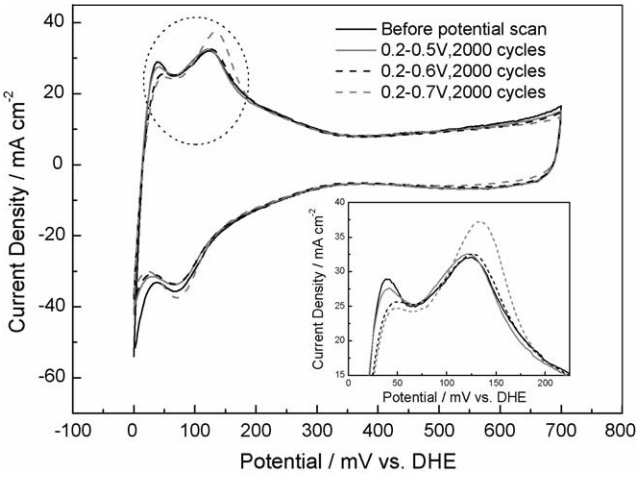

Fig. 1. CV curves of the electrocatalyst before and after potential scans. Scan rate: 20 mV s^{-1}; temperature: 60 °C.

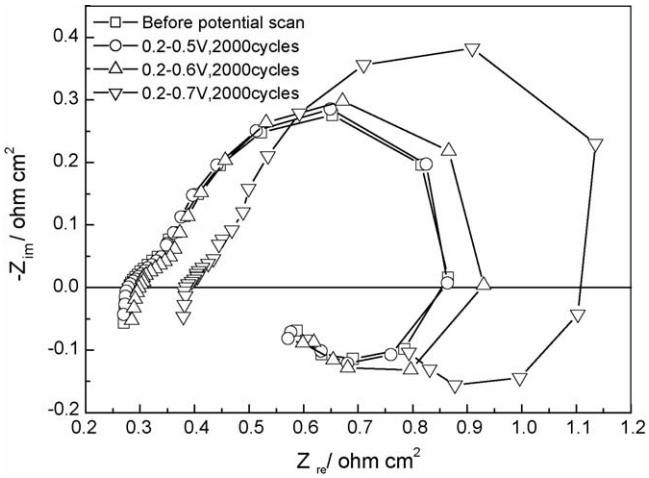

Fig. 3. Nyquist diagram of anode EIS at 0.4 V vs. DHE before and after potential scans. Anode feed: 1 mol L^{-1} methanol solution. Cathode feed: hydrogen at 0.1 MPa; temperature: 75 °C.

after a potential scan in the 0.2–0.6 V and 0.2–0.7 V regions, especially for the latter, which may be explained by the dissolution of hydrous ruthenium oxide from the catalyst layer, as discussed in the following contexts.

The methanol-stripping curves (Fig. 2) show the right-shift of the methanol adsorbate-oxidation peak with the extending scan region. Similar to Fig. 1, the right-shift also occurred after potential scans in 0.2–0.6 V and 0.2–0.7 V regions, and for the latter, the degree is much higher. For a Pt-rich PtRu electrocatalyst, the peak potential for methanol electro-oxidation shows a high value [22,23]. So the right-shift of the peak might also imply that part of the ruthenium dissolved from the electrocatalyst surface.

The anode impedance was determined in a three-electrode configuration with the PtRu/C anode, the working electrode and the hydrogen electrode the counter/reference electrode. The bias potential was held at 0.4 V. The anode chamber was fed with 1 mol L^{-1} methanol solution at a flow rate of 1 mL min^{-1}, while the cathode was fed with humidified hydrogen and served as a DHE, as described in the experimental section. The Nyquist diagram (Fig. 3) consists of two arcs. The arc which appears in the higher frequency range is independent of the potential change, and can be ascribed to the ionic resistance of the membrane in parallel with a capacitance relating to both the double layer capacitances and the geometric capacitance of the electrode [24,25]. The impedance of hydrogen evolution reaction in the counter electrode might also manifest itself in this arc. Pure ohmic resistance, including resistances of the electronically conducting cell components as well as contact resistances, can be derived from the intersection of the arc on real axis at the high-frequency end. The intersection of the high-frequency arc on the real axis at the low-frequency end is relevant to the ionic resistance of the membrane and the resistance of the hydrogen evolution reaction in the counter electrode. The arc which appears in the lower frequency range is dependent on the potential. It relates to the electro-oxidation of methanol, and at the low-frequency end, this arc extended into the fourth quadrant and formed an induction loop that represents the electro-oxidation of $(CO)_{ads}$ [25–28].

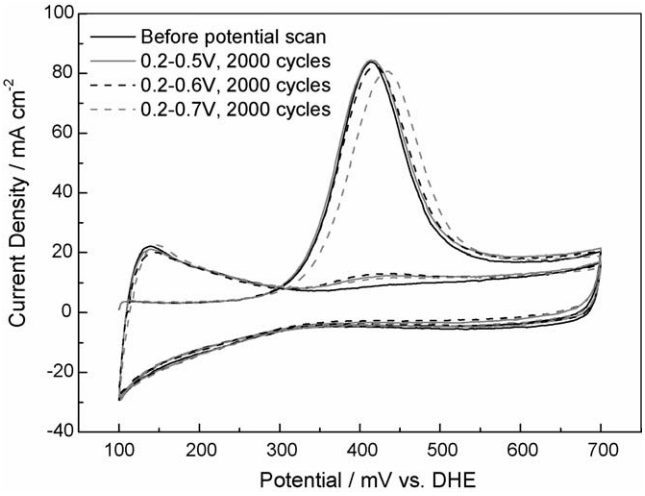

Fig. 2. Methanol-stripping curves before and after potential scans. Scan rate: 20 mV s^{-1}; temperature: 60 °C.

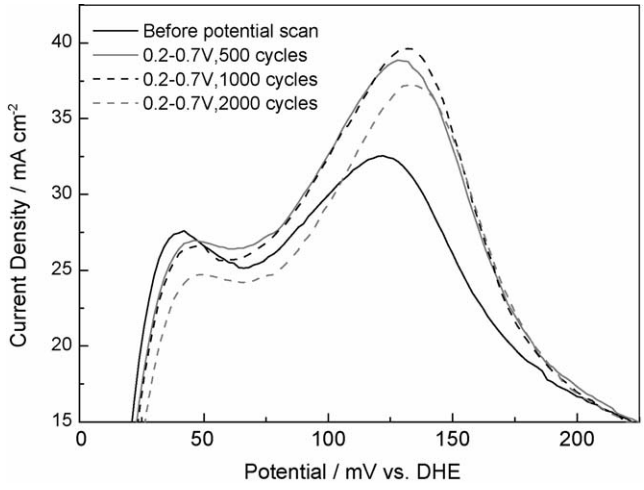

Fig. 4. CV curves of the electrocatalyst before and after potential scan in 0.2–0.7 V region. Scan rate: 20 mV s^{-1}; temperature: 60 °C.

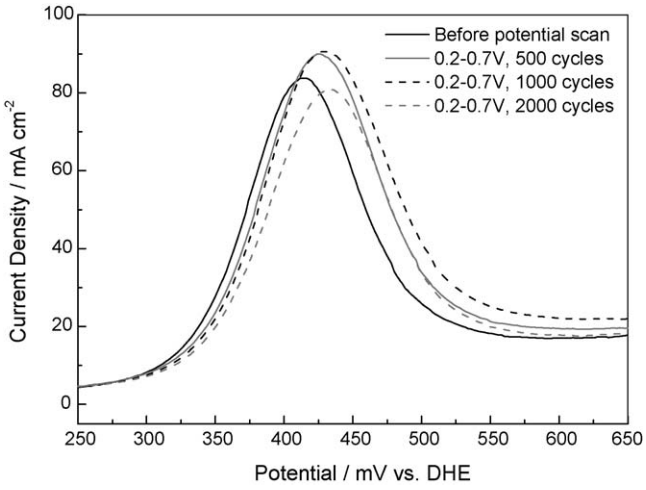

Fig. 5. Methanol-stripping curves before and after potential scan in 0.2–0.7 V region. Scan rate: 20 mV s^{-1}; temperature: 60 °C.

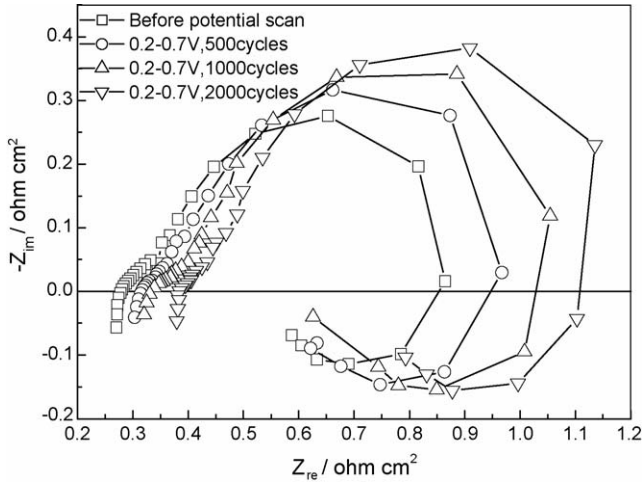

Fig. 7. Nyquist diagram of anode EIS at 0.4 V vs. DHE before and after potential scan in 0.2–0.7 V region. Anode feed: 1 mol L^{-1} methanol solution. Cathode feed: hydrogen at 0.1 MPa. Temperature: 75 °C.

Fig. 3 further confirmed the influence of the potential scan in the potential regions of 0.2–0.6 V and 0.2–0.7 V on the PtRu/C electrocatalyst. After potential scan in the 0.2–0.6 V and 0.2–0.7 V regions, especially the latter, both the pure ohmic resistance (intersection of high-frequency arc on the real axis) and the methanol electro-oxidation impedance (low-frequency arc) increased to some extent. The increase of the methanol electro-oxidation impedance may be caused by the variation of catalyst composition due to ruthenium loss. On the other hand, the increase of pure ohmic resistance can be ascribed to the enhanced contact resistance between the diffusion layer and the catalyst layer or between the catalyst layer and the membrane also due to ruthenium loss from the catalyst layer.

From the results listed above, it is suggested that, the potential scan in the 0.2–0.5 V region, which simulates the anode potential under normal operating conditions, does not influence the PtRu/C electrocatalyst, but when the upper limit of the potential region is elevated to 0.6 V or even higher, electrocatalyst degradation will take place.

In order to study the remarkable degradation of the PtRu/C electrocatalyst which occurred during the potential scan in the 0.2–0.7 V region in detail, results obtained after cycle numbers of 0, 500, 1000 and 2000 in this potential region are compared.

The hydrogen-desorption peaks in the CV curves are shown in Fig. 4. It is clearly seen that the hydrogen-desorption peak moved to the right with increase of cycle number. But interestingly, the peak area increased at the beginning, and reached a maximum value at the cycle number 1000, then began to decline. Methanol-stripping peaks (Fig. 5) also show a similar trend: with the cycle number increased, the methanol-stripping peak moved to the right, but the peak area reached its maximum value at the cycle number of 1000, then began to decline. The most probable reason for this phenomenon is that: at the beginning of the potential scan, the sudden dissolution of ruthenium left many small voids on the surface of the electrocatalyst, which made the catalyst surface coarse, with a high surface-area value. With the potential scan continuing, the small voids gradually vanished under the electrochemical stress.

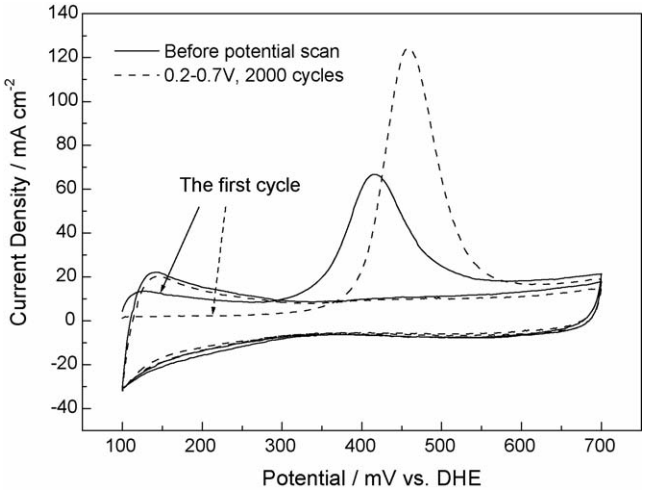

Fig. 6. CO-stripping curves before and after potential scan in 0.2–0.7 V region.

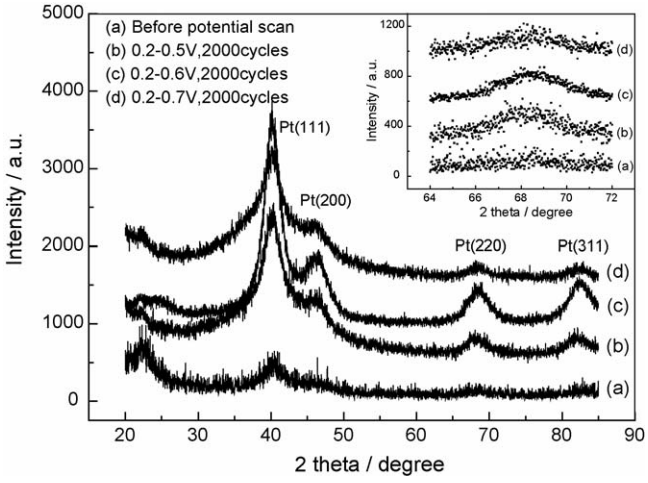

Fig. 8. XRD patterns of the electrocatalyst before and after potential scans.

The variation in catalyst composition manifests itself more remarkably in the CO-stripping curves (Fig. 6). After a potential scan in 0.2–0.7 V region, the CO electro-oxidation peak became more Pt-like [29–32]: in the first scan-cycle, when CO molecules were adsorbed onto the electrocatalyst, the hydrogen-desorption peak was almost completely suppressed; and the CO electro-oxidation peak became narrower with a significant right-shift in peak position. This result strongly supports the assumption that ruthenium dissolved dramatically from the electrocatalyst during the potential scan in the 0.2–0.7 V region.

The Nyquist diagram of anode EIS after potential scan in the 0.2–0.7 V region (Fig. 7) shows that both the ohmic resistance and the methanol electro-oxidation impedance increased monotonously with the scan cycle number. This result confirmed that a pronounced electrocatalyst degradation took place during the potential scan in the 0.2–0.7 V region.

The powder X-ray diffraction patterns of the anode catalyst layer before and after potential scans are shown in Fig. 8. The Pt (2 2 0) peak was selected to calculate the mean particle size of the electrocatalyst because it is isolated from the diffraction peaks of the carbon support and the Nafion® polymer electrolyte. The mean particle sizes were calculated according to Scherrer's formula [33]:

$$L = \frac{0.9\lambda_{k\alpha 1}}{B_{(2\theta)} \cos\theta_{\max}} \quad (1)$$

Table 1
Particle size of the PtRu/C electrocatalyst before and after potential scans

Electrocatalyst	XRD particle size (nm)	TEM particle size (nm)
Before potential scan	3.0	3.1
After scan in 0.2–0.5 V	3.0	3.2
After scan in 0.2–0.6 V	2.9	3.2
After scan in 0.2–0.7 V	3.0	3.5

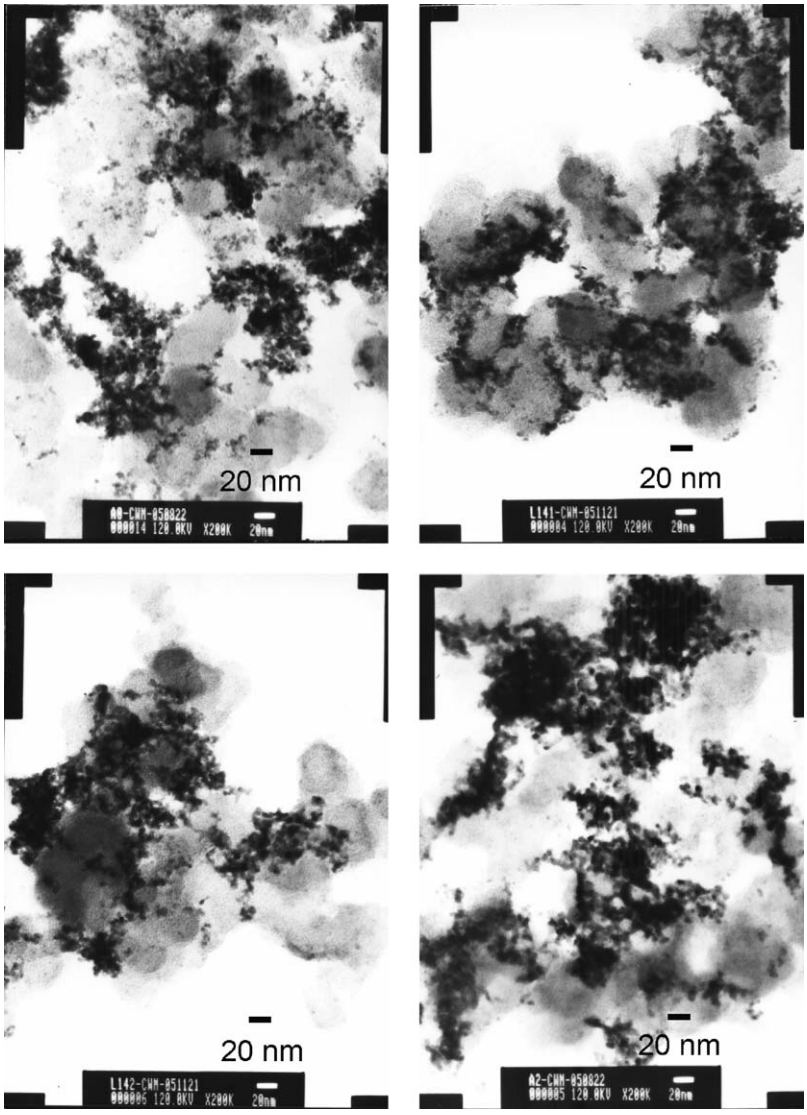

Fig. 9. TEM images of the electrocatalyst: (a) before potential scan, (b) after potential scan in 0.2–0.5 V region, (c) after potential scan in 0.2–0.6 V region and (d) after potential scan in 0.2–0.7 V region.

Table 2
EDX analysis of the anode catalyst layer before and after potential scans

Catalyst layer	C (wt.%)	O (wt.%)	Ru (wt.%)	Pt (wt.%)	Pt:Ru wt. ratio
Before potential scan	66	4	9	21	2.3
After scan in 0.2–0.5 V	68	4	9	19	2.2
After scan in 0.2–0.6 V	69	4	8	19	2.4
After scan in 0.2–0.7 V	74	3	6	17	2.8

where $\lambda_{k\alpha 1}$ is the wavelength of X-ray (1.5418 Å), θ_{max} the angle at the peak maximum, and $B_{2\theta}$ is the width (in radians) of the peak at half height.

The XRD results show that, the variation in particle size of the electrocatalyst during potential scans is negligible (Table 1). This fact may be explained as follows: ruthenium exists partly in the form of amorphous hydrous oxide, RuO_xH_y, which does not manifest itself in the XRD patterns. Compared with the metallic ruthenium incorporated into the face-centered cubic (fcc) lattice of platinum, amorphous ruthenium oxides have a stronger tendency to dissolve from the catalyst surface [10]. So the partial dissolution of ruthenium from the electrocatalyst could not be observed in the XRD patterns. The hydrous ruthenium oxide, RuO_xH_y, is a mixed electron/proton conductor [34–36]. Its loss leads to both an enhanced pure ohmic resistance and an increased charge-transfer impedance for methanol oxidation, as revealed by the Nyquist diagrams of anode EIS shown in Figs. 3 and 7.

From the TEM images (Fig. 9), it seems that after a potential scan in 0.2–0.7 V region, the catalyst particles grew to some extent. The apparent mean particle size increased from 3.1 nm to 3.5 nm (Table 1). But according to the XRD results, the "real" particle size did not change. So this phenomenon may be explained by the migration of catalyst crystallites under electrochemical stress.

The results of the EDX analysis obtained from the catalyst layer (Table 2) revealed two changes after a potential scan in 0.2–0.7 V region: the enhanced Pt/Ru weight ratio, and the increased carbon content. The former confirmed the dissolution of ruthenium from the electrocatalyst, and the latter likely suggests that part of catalyst crystallites migrated within the catalyst layer under electrochemical stress [7,37]. This explanation is also in consistent with the TEM images shown in Fig. 9.

4. Conclusions

For the direct methanol fuel cell, the anode potential is one of the most important factors that influences the stability of electrocatalysts. Compared with the cathode potential, the anode potential normally has a relatively weak influence on electrocatalysts. But in the case of deep discharge or short circuit, the anode potential value may exceed 0.6 V versus DHE, which is harmful to the anode electrocatalyst. The dissolution of anode catalyst components results in an enhanced ohmic resistance and a lowered catalytic activity for methanol electro-oxidation.

Acknowledgements

This work was financially supported by Samsung Advanced Institute of Technology (SAIT), Innovation Foundation of Chinese Academy of Sciences (K2003D2), National Natural Science Foundation of China (Grant No. 20173060), Hi-Tech Research and Development Program of China (2003AA517040) and Knowledge Innovation Program of the Chinese Academy of Sciences (KGCX2-SW-310).

References

[1] H. Dohle, H. Schmitz, T. Bewer, J. Mergel, D. Stolten, J. Power Sources 106 (2002) 313.
[2] A.S. Aricò, S. Srinivasan, V. Antonucci, Fuel Cells 1 (2001) 133.
[3] X. Ren, P. Zelenay, S. Thomas, J. Davey, S. Gottesfeld, J. Power Sources 86 (2000) 111.
[4] S. Wasmus, A. Küver, J. Electroanal. Chem. 461 (1999) 14.
[5] H.R. Colón-Mercado, H. Kim, B.N. Popov, Electrochem. Commun. 6 (2004) 795.
[6] H.R. Colón-Mercado, B.N. Popov, J. Power Sources 155 (2006) 253–263.
[7] P. Yu, M. Pemberton, P. Plasse, J. Power Sources 144 (2005) 11.
[8] N.P. Lebedeva, G.J.M. Janssen, Electrochim. Acta 51 (2005) 29.
[9] A. Taniguchi, T. Akita, K. Yasuda, Y. Miyazaki, J. Power Sources 130 (2004) 42.
[10] P. Piela, C. Eickes, E. Brosha, F. Garzon, P. Zelenay, J. Electrochem. Soc. 151 (2004) A2053.
[11] X. Ren, T.E. Springer, S. Gottesfeld, J. Electrochem. Soc. 147 (2000) 92.
[12] M.K. Ravikumar, A.K. Shukla, J. Electrochem. Soc. 143 (1996) 2601.
[13] W.L. Holstein, H.D. Rosenfeld, J. Phys. Chem. B 109 (2005) 2176.
[14] M.S. Wilson, S. Gottesfeld, J. Appl. Electrochem. 22 (1992) 1.
[15] W.F. Lin, M.S. Zei, M. Eiswirth, G. Ertl, J. Phys. Chem. B 103 (1999) 6968.
[16] T. Iwasita, H. Hoster, A. John-Anacker, W.F. Lin, W. Vielstich, Langmuir 16 (2000) 522.
[17] H. Hoster, T. Iwasita, H. Baumgärtner, W. Vielstich, J. Electrochem. Soc. 148 (2001) A496.
[18] E.M. Crabb, M.K. Ravikumar, D. Thompsett, M. Hurford, A. Rose, A.E. Russell, Phys. Chem. Chem. Phys. 6 (2004) 1792.
[19] G.A. Camara, R.B. de Lima, T. Iwasita, Electrochem. Commun. 6 (2004) 812.
[20] D. Chu, S. Gilman, J. Electrochem. Soc. 143 (1996) 1685.
[21] D. Cao, S.H. Bergens, Electrochim. Acta 48 (2003) 4021.
[22] Z. Jusys, J. Kaiser, R.J. Behm, Electrochim. Acta 47 (2002) 3693.
[23] Z. He, J. Chen, D. Liu, H. Zhou, Y. Kuang, Diam. Relat. Mater. 13 (2004) 1764.
[24] J.T. Mueller, P.M. Urban, J. Power Sources 75 (1998) 139.
[25] J. Otomo, X. Li, T. Kobayashi, C. Wen, H. Nagamoto, H. Takahashi, J. Electroanal. Chem. 573 (2004) 99.
[26] J.T. Müller, P.M. Urban, W.F. Hölderich, J. Power Sources 84 (1999) 157.
[27] I.M. Hsing, X. Wang, Y.J. Leng, J. Electrochem. Soc. 149 (2002) A615.
[28] T. Vidaković, M. Christov, K. Sundmacher, Electrochim. Acta 49 (2004) 2179.

[29] F. Maillard, G.Q. Lu, A. Wieckowski, U. Stimming, J. Phys. Chem. B 109 (2005) 16230.
[30] J.C. Davies, B.E. Hayden, D.J. Pegg, M.E. Rendall, Surf. Sci. 496 (2002) 110.
[31] H.N. Dinh, X. Ren, F.H. Garzon, P. Zelenay, S. Gottesfeld, J. Electroanal. Chem. 491 (2000) 222.
[32] C. Bock, B. MacDougall, Y. LePage, J. Electrochem. Soc. 151 (2004) A1269.
[33] V. Radmilović, H.A. Gasteiger, P.N. Ross, J. Catal. 154 (1995) 98.
[34] D.R. Rolison, P.L. Hagans, K.E. Swider, J.W. Long, Langmuir 15 (1999) 774.
[35] J.W. Long, R.M. Stroud, K.E. Swider-Lyons, D.R. Rolison, J. Phys. Chem. B 104 (2000) 9772.
[36] W. Dmowski, T. Egami, K.E. Swider-Lyons, C.T. Love, D.R. Rolison, J. Phys. Chem. B 106 (2002) 12677.
[37] J. Xie, D.L. Wood, K.L. More, P. Atanassov, R.L. Borup, J. Electrochem. Soc. 152 (2005) A1011.